ELSEVIER

Journal of Magnetism and Magnetic Materials 200 (1999) 405–424

Journal of magnetism and magnetic materials

www.elsevier.com/locate/jmmm

Magnetic nitrides

J.M.D. Coey*, P.A.I. Smith

Physics Department, Trinity College, Dublin 2, Ireland

Received 10 March 1999

Abstract

Nitrogen enters 3d metals and 3d–4f intermetallic compounds as an interstitial provoking a dilation of the lattice. Iron-based alloys are most susceptible to modification by nitrogen, which can turn them from weak to strong ferromagnets. In the 3d–4f compounds it is a major contributor to the crystal field. The influence of nitrogen in BCC, FCC and HCP iron, and then in iron-based intermetallics with 2 : 17, 1 : 12 and 3 : 29 structure types is reviewed. Important issues are the role of nitrogen in enhancing the iron moment and raising the Curie temperature. Progress in processing nitrogen-containing compounds is outlined, and applications of iron nitrides as permanent magnets and as materials for use in magnetic recording are discussed.

Keywords: Iron nitrides; Thin films; Ferromagnetism; Magnetic recording; Rare-earth permanent magnets; Intermetallic compounds; Nitrogenation; Crystal field

1. Introduction

A few light elements at the beginning of the periodic table are small enough in their covalent or metallic state to enter the lattice of the magnetic 3d metals interstitially. These elements are principally hydrogen, boron, carbon and nitrogen. Oxygen, fluorine and chlorine are so strongly electronegative that they tend to form negative ions. Of course, size is but one of the factors governing solubility — hydrogen, the smallest interstitial, is essentially insoluble in iron, whereas carbon dissolves in both α and γFe to yield the most versatile and useful series of alloys known to man. Nitrogen is a diatomic gas in normal conditions, like hydrogen, but unlike carbon and boron which have very high melting points (> 2500 K). The usual approach to form nitrides and nitrogen-containing compounds is gas-phase interstitial modification, which is quite different to the melting of elements or prealloys employed with carbon or boron. The temperatures used may be quite low (~ 670 K) and there is an opportunity to form and retain non-equilibrium phases at room temperature when the decomposition kinetics are interminably slow. High nitrogen pressures may be used, or high effective pressures achieved by using a nitrogen-containing gas such as ammonia [1]. Thin films can be prepared by methods such as reactive sputtering in an Ar/N_2 mixture or ion implantation.

As an interstitial impurity, nitrogen tends to dilate the host lattice. In magnetism, maximum interest is focused on iron and iron-based alloys because these materials are of greatest practical use. Iron has the highest ferromagnetic polarisation at room temperature (2.15 T) and it is by far the cheapest

* Corresponding author. Tel.: + 353-1-608-1470; fax: + 353-671-1759.

E-mail address: jcoey@tcd.ie (J.M.D. Coey)

0304-8853/99/$ - see front matter
PII: S0304-8853(99)00429-1

magnetic element. The magnetic properties of iron are volume-sensitive, with a critical interplay between structure and magnetism. The normal body-centred cubic (BCC) phase αFe is a weak ferromagnet with a zero-temperature moment of 2.22 μ_B/atom and a Curie temperature of 1044 K. A moment of 2.7 μ_B/atom would be expected if iron were a strong ferromagnet, with the 3d↑ states fully occupied. Since γFe is unstable at room temperature, the phase must be stabilised, for example as thin films on an FCC substrate such as copper or at grain boundaries. The magnetic properties of face-centred cubic (FCC) γFe are particularly sensitive to lattice volume, and states may be found which have a high moment, a low moment or are non-magnetic according to the lattice parameter. Many magnetic alloys of practical interest are cubic solid solutions of iron, with cobalt or nickel, for example. Iron can also be stabilised in a ferromagnetic hexagonal close-packed ε phase under suitable conditions.

There are numerous iron-rich intermetallic compounds, but those of greatest interest in magnetism involve the 4f rare-earth elements. Typically, the iron lattice in these intermetallics approximates a close-packed structure. Compounds such as $Nd_2Fe_{14}B$ are stabilised by interstitial boron. Others such as Sm_2Fe_{17} have interstices in their structure which can be occupied by hydrogen, carbon or nitrogen, sometimes with dramatic consequences for the magnetic properties [2].

In developing practically useful magnetic materials operating at room temperature it is often desirable to combine the greatest-possible polarisation with either negligible coercivity in a soft material or high coercivity in a hard material. Other considerations such as Curie temperature, magnetostriction, resistivity, mechanical properties and corrosion resistance may also be critically important and no material is perfect in every respect. For example, the disordered FCC $Fe_{20}Ni_{80}$ alloy, permalloy, is an excellent soft magnetic material used in many thin film applications because it combines low anisotropy and negligible magnetostriction. By a happy coincidence in the $Fe_{100-x}Ni_x$ series, K_1 and λ_s change sign at almost the same composition, 0.75 and 0.82, respectively, depending somewhat on heat treatment. Unfortunately the polarisation of permalloy is only 1.0 T. Likewise, $Nd_2Fe_{14}B$ is a versatile high-performance permanent magnet material but its polarisation (1.61 T) and Curie temperature (585 K) both leave something to be desired.

Interstitial nitrogen has the potential to alter the properties of iron-based alloys in a useful sense, and it may be combined with substitutions or other interstitials to achieve an optimum set of properties for a particular application. Here we focus on the effects of incorporating nitrogen in iron, and some iron-based intermetallics in order to illustrate the main effects of nitrogen on the magnetic properties. We refer to all these materials as 'nitrides', although they do not necessarily possess a fixed stoichiometry.

2. Iron nitrides

All ordered iron nitrides are metastable compounds, which can persist at moderate temperatures because of kinetic constraints. We consider in turn phases related to α, γ and εFe.

2.1. αFe-N

Equilibrium solubility of interstitial nitrogen in BCC iron reaches a maximum of just $x = 0.4$ at% at 860 K. The lattice dilation in $\alpha Fe_{100-x}N_x$, $d(\ln V)/dx$ is ~ 0.002 [3], and there is a change of magnitude of the ^{57}Fe hyperfine field of -3 T/% [4]. More nitrogen can be incorporated into the BCC lattice of thin films prepared by reactive sputtering or ion implantation. The cubic films may accommodate up to 10 at% nitrogen, with a nonuniform profile across the film thickness [5]. They have a microcrystalline structure with possible secondary $\gamma' Fe_4N$ and $\alpha'' Fe_{16}N_2$. Their polarisation has been reported to be similar to, or slightly higher than that of αFe [6–8], or else to be significantly higher, 2.4–2.5 T [5,8,9]. The metastable cubic phase is also denoted as α''' or α^* [6]. As-deposited films with high nitrogen content often contain the tetragonal α' phase (nitrogen martensite) discussed below.

Substituting a few percent ($\sim$ 2–3%) of an element X (Al, Ta, Ti, Rh, ...) which increases the

solubility of nitrogen or extends the stable α-phase field, leads to nitride films with very interesting soft magnetic properties. The substitutions in αFe-X-N also inhibit grain growth, stabilizing the soft magnetic properties associated with anisotropy averaging in systems of tiny particles to higher temperatures [10,11]. There can be a reduction in the cubic anisotropy constant from the value of 48 kJ/m^3 for pure iron to less than 0.5 kJ/m^3 for suitably prepared films. The polarisation remains close to 2 T, and the saturation magnetostriction λ_s, which is -9×10^{-6} in pure iron, changes sign at about 3 at% nitrogen [12]. The low-anisotropy/low magnetostriction BCC iron-based films are attractive candidate materials for inductive thin film write heads in magnetic recording. Currently these are made of permalloy, sendust ($Fe_{74}Al_{10}Si_{16}$), a nonmagnetostrictive amorphous alloy of typical composition $Co_{90}Zr_5Nb_5$, or $Fe_{55}Ni_{45}$ which have a polarisation of 1.0, 1.1, 1.4 and 1.6 T, respectively. A polarisation approaching 2 T is needed to create sufficient stray field to write on the higher-coercivity media (H_c = 300–400 kA/m) which are needed as head and bit dimensions decrease to allow recording densities in excess of 10 bits/μm^2 (7 Gbits/in^2) [10]. In addition, to accommodate high data transfer rates, a good high-frequency magnetic response is required up to a frequency of 100 MHz.

The rapid change in magnetostriction with nitrogen content was first attributed to the presence of $\gamma'Fe_4N$ in exchange-coupled nanocomposites [7], but it has since been shown to be an intrinsic property of αFe with interstitial nitrogen [3,12]. The presence of $\gamma'Fe_4N$ in the films is detrimental, and it is suppressed for example by Ta [11] or Ti [14] substitution. $\gamma'Fe_4N$ in the films has $\lambda_s<0$, like αFe. Recent work on films with a ⟨1 1 0⟩ fibre texture shows that it is the $\lambda_{1\,1\,1}$ cubic magnetostriction constant that increases monotonically from -20×10^{-6} with increasing nitrogen, while $\lambda_{1\,0\,0}$ remains practically constant at 20×10^{-6} [13]. The polycrystalline average λ_s then changes sign at $x=3$ [12].

In order to stabilise the domain structure in the heads, it is necessary to impose a direction of easy magnetisation parallel to the airgap. This may be achieved by magnetic annealing, or by sputtering αFe–X–N films in a small transverse magnetic field. The nitrogen has a tendency to align in planes perpendicular to the applied field. The value of the induced anisotropy K_u is a few hundred J/m^3 and in order to stabilise the induced anisotropy, nitrogen diffusion has to be suppressed. Lamination of the BCC iron nitride films with permalloy, SiO_2, SiN or AlN is useful [15–18]; it reduces coercivity to 40 A/m, and improves the high-frequency response of the relatively thick films (∼1 μm) needed for heads [16].

2.2. α′Fe–N

Another approach to preparing a nitrogen-rich alpha phase is to quench γFe–N so that it will transform martensitically into the tetragonal α′ nitrogen martensite. The greatest solubility of N in γFe is $x=10.5$ at%, at 920 K. Typically, the martensitic transformation is incomplete, and the resulting bulk material is a mixture of tetragonal nitrogen martensite and γFe–N. The nitrogen in the α′ phase is disordered, and it induces a lattice expansion $\mathrm{d}(\ln V)/\mathrm{d}x$ of 0.006; $\mathrm{d}(c/a)\mathrm{d}x=0.01$. There is a continuous range of composition $1<x<10$. Based on a quantitative phase analysis, the magnetisation of bulk $\alpha'Fe_{100-x}N_x$ with $x\approx10$ is reported to be 250(10) Am^2/kg ($\mu_0M=2.4(1)$ T) [19].

Epitaxial thin films of the α′ phase can be prepared directly by MBE [20], reactive sputtering [21], ion-beam deposition [22] or by nitrogen ion implantation [23]. The polarisation of the α″ phase is reported to be 2.2–2.3 T [21,22], or 2.4 T [20], significantly higher than that of αFe. Due to the nitrogen disorder, a distribution of hyperfine fields appears [4,21], with three broad peaks associated with iron having 0, 1 or 2 nitrogen nearest-neighbours [4].

2.3. α″$Fe_{16}N_2$

Prolonged annealing (tempering) of the α′ phase at about 370–420 K leads to an ordering of the nitrogen to produce the famous ordered nitrogen martensite $\alpha''Fe_{16}N_2$, first described by Jack in the early 1950s [3]. The unit cell with $a=572$ pm and $c=629$ pm is doubled in all three directions, as

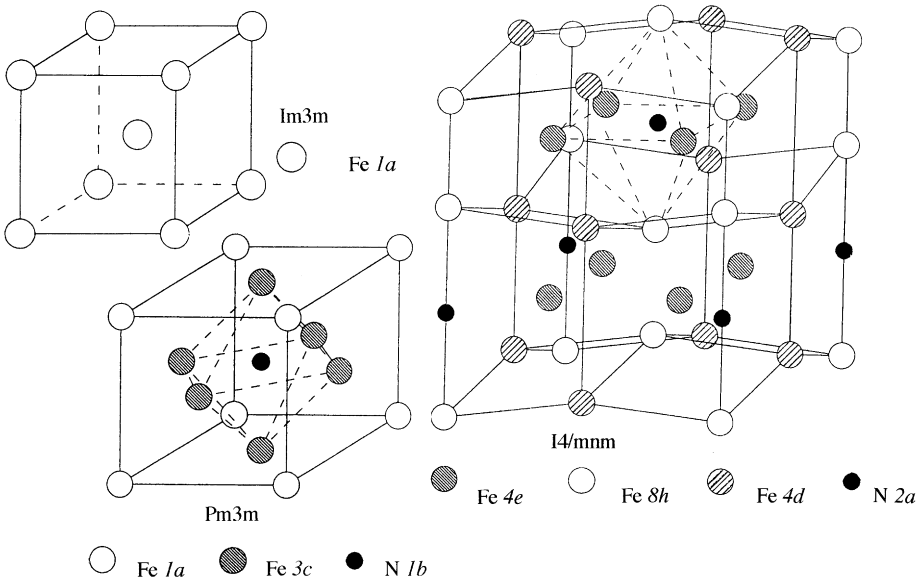

Fig. 1. Crystal structures of αFe, γ′Fe_4N and α″$Fe_{16}N_2$, drawn to scale.

illustrated in Fig. 1. The structure was recently refined by electron diffraction [25]. There are three inequivalent sites, 4d (mm2) with no nitrogen neighbour, 4e (4mm) with one nitrogen neighbour at 193 pm, and 8h (mm) with two nitrogen neighbours at 179 pm. The ordering is constrained by strain which develops as the nitrogen diffuses to form the α″ phase, which may have nitrogen vacancies [24]. Prolonged annealing or higher temperature treatment leads to decomposition of the α″ compound into αFe and γ′Fe_4N. The limited solubility of nitrogen in γFe, at most 10.5 at%, means that it is impossible to obtain a pure 16 : 2 phase (11.1 at%) by the quench and anneal route. Bulk samples containing 30–60% α″$Fe_{16}N_2$ have been produced in this way [19,26,27]. Much larger amounts of the α″ phase ($\gtrsim$80%) can be stabilised in thin films grown by MBE [20,28–30], reactive sputtering [6,21], ion implantation [23,31] or ion-beam deposition [32,33].

Interest in the magnetic properties of the α″ phase dates from the work of Kim and Takahashi on iron films evaporated in nitrogen [34]. Their films were a mixture of αFe and the α″ phase, and the polarisation of α″$Fe_{16}N_2$ was inferred to be as high as 2.8 T, corresponding to an average iron moment of 3.0 μ_B. Many groups have subsequently investigated the magnetic properties of the bulk and thin film samples containing this iron nitride. Much of the work was reviewed in symposia at MMM conferences (J. Appl. Phys. 76, 6620–55; 79, 5564–81). Research was stimulated by the reports of very large moments by Sugita et al. for single-crystal thin films grown epitaxially on GaAs or ($Ga_{0.8}In_{0.2}$)As by MBE. [20,28,29]. Moments are found to be as high as 3.5 μ_B/Fe [30], with a corresponding polarisation of 3.2 T. These films were about 50 nm thick, with $\sim$11 at% nitrogen. They were annealed for a prolonged period at 470 K in a vacuum of 10^{-8} torr to produce the α″ phase.

The repeated claim by the Hitachi group [30] and others [35] of a moment far in excess of that corresponding to strong ferromagnetism of iron on the Slater–Pauling curve (2.7 μ_B) caused a considerable stir, and led to an extended effort to confirm or deny the result.

2.3.1. Electronic structure calculations

Many groups have carried out electronic structure calculations. Most of these use the local spin density approximation (LSDA), and many make the atomic spheres approximation (ASA), although

there are some first-principles calculations using the full-potential augmented plane wave method [38,40], and nonlocal corrections have been evaluated using the generalised gradient approximation [37]. There is a good measure of agreement among the results of the different band calculations, which moreover yield reasonable values for the moment on iron itself and the moments on Fe_4N. Ten of these calculations were summarised by Sakuma [38], and some others [39–42]. The results of all 14 calculations taken together give the following site moments in μ_B, where the standard deviations are given in brackets: 4e-2.10(19), 8h-2.35(19), 4d-2.90(20), N- − 0.02(4). The average moment per iron is therefore 2.45(15) μ_B. Orbital contributions to the moment are generally found to be $< 0.1\ \mu_B$, as in αFe. The corresponding polarisation is 2.22(14) T.

The effects of introducing nitrogen into iron are (i) to change the 3d density of states, and reduce the difference in occupancy of the 3d↑ and ↓ states due to hybridisation with the sp orbitals of nitrogen, (ii) to expand the lattice, reducing the 3d–3d overlap, and hence the bandwidth, which tends to make iron a strong ferromagnet, and (iii) to change the symmetry of the iron sites. Kanamori [43] explained why there is a reduced moment on the iron sites that are the nearest-neighbours of nitrogen, and an enhanced moment on the more distant sites (1a in Fe_4N, 4d in $Fe_{16}N_2$, 6c and 9d in $Y_2Fe_{17}N_3$). The process is illustrated in Fig. 2. Hybridisation of the 3d states of the iron that is a nearest neighbour with the nitrogen sp states reduces the spin splitting, and especially lowers the potential for 3d↓ electrons. There is then charge transfer from the more distant iron, predominantly from 3d↓ to 3d↓ states. This depletes the 3d↓ band of the strongly ferromagnetic distant neighbours, and increases their moment above 2.7 μ_B. The mixing and charge-transfer process however, cannot increase the *average* iron moment above 2.7 μ_B. These ideas are borne out by a comparison of the calculated moments in $Fe_{16}X_2$, where X = vacancy or N [38,41], which allow the lattice expansion and hybridisation effects to be separated.

2.3.2. Bulk samples

Bulk samples obtained by quenching nitrogen austenite, and then annealing the martensite to produce the ordered α″ phase contain 30–60% of the α″ phase [36]. Deducing the magnetisation requires quantitative phase analysis, based on the X-ray diffraction or Mössbauer spectroscopy, since αFe and γFe as well as γ′Fe_4N and a highly disordered phase may be present [24–26]. The room-temperature magnetisation of the α″ phase deduced in this way by averaging data for 25 samples is $\sigma = 251(28)\ Am^2/kg$, corresponding to an average moment of 2.58(29) μ_B/Fe and a polarisation of 2.35 T. It is worth mentioning that the magnetisation in none of the multiphase samples was appreciably greater than that of αFe. Furthermore, the heat treatment to order the nitrogen in the martensite produces little change in the total magnetisation, with increases or decreases of a few percent being reported [26,45]. This seems to rule out the idea that a large moment may be associated with some intermediate degree of order.

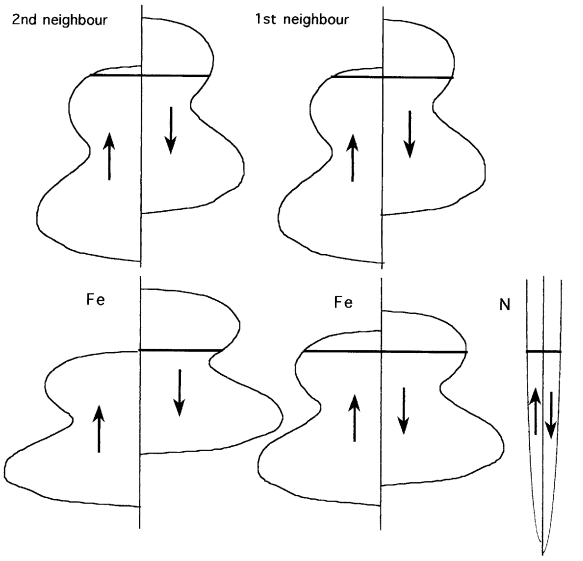

Fig. 2. Schematic changes in the electronic structure at first and second neighbour iron sites, induced by hybridisation with nitrogen.

2.3.3. Hyperfine fields

Hyperfine fields have been measured by ^{57}Fe Mössbauer spectroscopy and NMR. In well-ordered α″$Fe_{16}N_2$, three hyperfine patterns are observed, with a 1 : 2 : 1 intensity ratio, corresponding to the three iron sites in the structure (Fig. 1). Here

the results on bulk specimens and thin films (with the exception of the MBE films of Sugita et al. [28]) are in good agreement. Averaging six sets of results [6,19,24,44–46] gives the following low-temperature hyperfine fields in tesla: 4e-30.3(4), 8h-32.4(5), 4d-41.5(5), with an average of 34.2(5). The room-temperature values are about 3% lower. In order to infer the iron moment, it is necessary to know the hyperfine 'constant' A. The value for αFe is $A = 15\ \mathrm{T}/\mu_B$, whereas that for γFe_4N is $12\ \mathrm{T}/\mu_B$. Since $\alpha''Fe_{16}N_2$ is chemically and structurally intermediate between the two (Fig. 1) a plausible choice is $13.5\ \mathrm{T}/\mu_B$, which gives an average iron moment of 2.53(15) μ_B, and a moment of 3.07(19) μ_B on the 4d site. The error here takes account of some uncertainty in A. The hyperfine constant for the Fermi contact term in the hyperfine interaction estimated from the local spin density approximation calculations is $11.1\ \mathrm{T}/\mu_B$, but it is known that these calculations systematically underestimate the hyperfine field by 5 T [39], which brings A up to $13.2\ \mathrm{T}/\mu_B$.

An egregious exception is the Mössbauer spectrum of the high-moment films of Sugita et al. [30], which have a single αFe-like spectrum with $B_{hf} = 33$ T, and show no sign of distinct subspectra for the three sites of the α″ structure. The hyperfine constant there would have to be $10.3\ \mathrm{T}/\mu_B$.

2.3.4. Thin films

Following the work of Kim and Takahashi [34] thin films containing large proportions of the α″ phase have been studied by many groups [47]. A systematic study of sputtered films by Takahashi et al. [6] led to the conclusion that the magnetisation of the α″ phase at room temperature did not exceed 240 Am^2/kg (2.47 μ_B/Fe), and that there was no strong correlation between the nitrogen ordering and magnetic moment. Films prepared by ion implantation gave an average moment per iron of 2.54 μ_B [48]. Somewhat higher moments have been reported in films prepared by ion beam deposition, reaching a value of 2.9 μ_B for the thinnest films (28 nm) [35].

The moments of the MBE-grown films of the Hitachi group are in a class of their own. Values deduced from magnetisation measurements of 34 nm thick films are reported as 3.3–3.5 μ_B at room temperature [30]. The epitaxial films show a large c-axis anisotropy and the anisotropy field may be estimated from ferromagnetic resonance data as approximately 1 T [30,33].

There are some accounts of the effects of substitutions on the stability and magnetisation of the α″ phase [49]. Ti, for example, increases its thermal stability [50], whereas Co diminishes it [51].

2.3.5. Discussion

It is difficult to rationalise the reports of giant magnetic moments in 3d alloys and interstitial compounds such as $\alpha''Fe_{16}N_2$ in terms of normal ideas of electronic structure. Extrapolating the Slater–Pauling curve gives an atomic moment for strongly-ferromagnetic iron of 2.7 μ_B. Applying the magnetic valence model of strong ferromagnetism [52] to the iron nitrides, assuming a valence of 2 for iron and -3 for nitrogen, and taking the number of iron sp electrons of either spin as 0.7, gives an average moment per iron of 2.4 μ_B for Fe_8N, 2.1 μ_B for Fe_4N and 1.9 μ_B for Fe_3N. All that is involved here is counting the electrons, assuming a full $3d^5\uparrow$ sub-band, no spin polarisation of the sp band and no orbital moment. Any reports of giant moments such as 3.5 μ_B/Fe in thin films of $\alpha''Fe_{16}N_2$ [30], 2.0 μ_B/atom in nanocrystalline electrodeposited $Fe_{23}Co_{65}Ni_{12}$ [53] or 3 μ_B/Fe in tiny iron clusters [54], need to be examined very critically as regards the magnetisation measurement itself. But if these claims stand up to scrutiny (and after ten years the Hitachi results have not been reproduced anywhere else), the common feature of all the high-moment systems seems to be the reduced dimensionality, and a high surface or interface to volume ratio. Although recent measurements on the interface or grain-boundary phases in iron [55] or amorphous Fe–N [56] do not support the conjecture of an elevated magnetic moment, there remains a possibility that narrow, spin–split sp states enhance the moment at the surface or interface, perhaps whenever there is coexistence of BCC and FCC phases. It is a practical challenge for the next century to produce bulk magnetic material with a room-temperature polarisation in excess of 2.45 T, perhaps by aggregating somehow tiny regions which do have an enhanced moment. Iron and nitrogen still look like a promising combination.

2.4. $\gamma' Fe_4N$

The simplest ordered Fe–N compound is cubic $\gamma' Fe_4N$ (Fig. 1). The FCC lattice is expanded by 33% by interstitial nitrogen in the 1b body centre position, giving a lattice parameter of 379.5 pm, compared with 345.0 pm for γFe; $d(\ln V)/dx = 0.017$. There are two inequivalent iron sites; the body-corner 1a site with cubic symmetry having 12 iron neighbours at 268 pm, and the 3c face-centre site with two nitrogen neighbours at 190 pm and 12 iron second neighbours at 268 pm.

The nitrogen-induced expansion stabilises a ferromagnetic state for γFe_4N with a Curie temperature of 767 K. At room temperature, the polarisation is 1.9 T ($\sigma = 210\ Am^2/kg$). The easy directions of magnetisation are ⟨1 0 0⟩. The moment at low temperature corresponds to 8.8 μ_B/formula, or an average of 2.2 μ_B/Fe. The different moments on the two crystallographic sites have been measured by neutron diffraction [57], or deduced from the ^{57}Fe hyperfine fields [42,58]. The 1a site has cubic symmetry (m3m), and an iron moment of 2.98 μ_B, whereas the 3c site has tetragonal symmetry (4/mmm) and a moment of 2.01 μ_B. The ⟨1 0 0⟩ easy directions of magnetisation are deduced from the quadrupole splitting of the 3c site Mössbauer spectrum; there are two subspectra, with intensity ratio 2 : 1 and quadrupole shifts in the ratio − 1 : 2, which are due to the two possible angles (90°, 0°) between the magnetisation direction and the local tetragonal N–Fe–N axis, which is the principal axis of the electric field gradient.

Numerous electronic structure calculations have been carried out for $\gamma' Fe_4N$. Some results are summarised in Table 1, and detailed references are to be found in Refs. [36,37,59]. There is good agreement between the calculations and the experimental results. The reason why the moments on iron sites which have nitrogen nearest-neighbours is reduced, and the second-neighbour iron moments is enhanced is given by Kanamori [43], and explained in Fig. 2.

A series of transition metal nitrides Fe_3MN form with the antiperovskite structure, where the 1c site may be occupied by Mn, Ni, Pd or Pt. The ordered compounds are ferromagnetic [60], whereas Mn_4N is ferrimagnetic [61].

Table 1
Magnetic properties of iron nitrides

			a (pm)	c (pm)	$m@T=0$ (μ_B/Fe)	$B_{hf}@T=0$ (T)	$\mu_0 M@$RT (T)	T_C (K)	K_1 (kJ/m^3)	λ_s ($\times 10^6$)
αFe			286.6		2.22	33.8	2.16	1044	48	− 9
$\alpha Fe_{97}N_3$	ms		287				2.2(1)			∼ 0
$\alpha' Fe_{90}N_{10}$	ms		283	312			2.3(1)			
$\alpha'' Fe_{16}N_2$	mc	4d	572	629	2.90*	41.5	2.3(1)	810	∼ 1000	
		4e			2.35*	30.3				
		8h			2.10*	32.4				
		av			2.35*	34.2				
$\gamma' Fe_4N$	qc	1a	379.5		2.98	36.6	1.8	767		− 10
		3c			2.01	23.5				
		av			2.25	26.8				
εFe_3N	qc		269.5	436		26.0		567		
ζFe_2N	qc		483.0	442.5	0.05	0.8		9		
			$b = 552.3$							
FeN(ZnS)	mc		433		–	–				
FeN(NaCl)	mc		450		5.0$^+$	49				
					3.0$^+$	30				

Note: ms: metastable solid solution, mc: metastable compound, qc: quasi-stable compound
*Calculated value.
$^+$ Estimate.

2.5. Other iron nitrides

The hexagonal εFe_3N phase has an extended homogeneity range, with a moment that decreases rapidly with increasing iron content. The stoichiometric compound is ferromagnetic, with $T_c = 567$ K. Iron occupies a single 6c site, with two nitrogen nearest-neighbours in 1d and 1e sites of the P312 space group. The moment is 1.9 μ_B [62]. Orthorhombic ζFe_2N has a similar iron packing, with different nitrogen order. Mössbauer spectra indicate that it orders below 9 K, with a tiny hyperfine field of 0.8 T [63]. It is possibly a very weak itinerant ferromagnet.

Metastable cubic nitrides, containing nearly 50 at% N, and having the ZnS or NaCl structures, can be synthesised by sputtering [63–65]. The ZnS-type nitride has been shown to be a non-magnetic metal, while the NaCl-type nitride is an antiferromagnet, with large magnetic hyperfine fields of 49 and 30 T at 4.2 K which suggest it should be regarded as an ionic compound. The two fields are associated with an ordered defect structure, the composition of the film containing the NaCl structure being $FeN_{0.63}$ [62].

A noncrystalline Fe–N phase has been produced by ball milling Fe_4N with αFe [56]. The material is ferromagnetic with a reduced magnetisation, and it was suggested that it forms in the grain boundaries of nanocrystalline αFe–N. The system may be recrystallised into its constituents by annealing at 470 K. By analogy with other 3d-metalloid amorphous systems, the likely composition is $Fe_{80}N_{20}$.

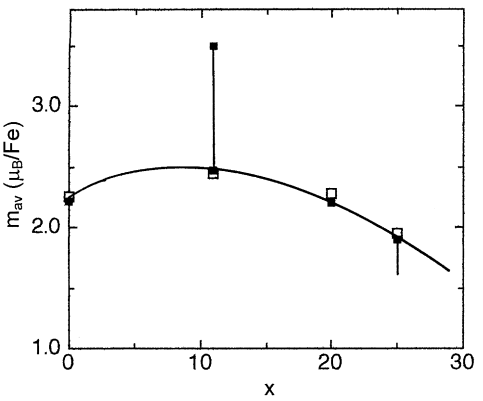

Fig. 3. Calculated (open symbol) and measured (solid symbol) average iron moments in Fe–N compounds.

A summary of the calculated and measured moments of iron–nitrogen compounds is shown in Fig. 3. Apart from some of the reports for $\alpha''Fe_{16}N_2$, there is rather good agreement. The intrinsic properties of the iron nitrides discussed are summarised in Table 1. Although the emphasis here has been on intrinsic magnetic properties, thin film applications will often depend critically on nanostructure, especially to achieve exchange averaging of the anisotropy needed for very soft material [66].

3. Nitrides of 3d–4f intermetallics

Following the discovery in 1990, by Coey and Sun [67], that the Curie temperature and anisotropy field of $Sm_2Fe_{17}N_{3-\delta}$ were superior to those of $Nd_2Fe_{14}B$, most interest in 3d–4f nitrides has focused on the series $R_2Fe_{17}N_y$. This led to investigation of other intermetallics which in their unmodified form were unsuitable for permanent magnet applications, such as the $ThMn_{12}$-type compounds $R(Fe_{12-x}M_x)$ and the $R_3(Fe_{29-x}M_x)$ compounds (where M = Ti, Mo, V, Cr). Skomski [1], Fujii and Sun [68] and Kobayashi [69] review $R_2Fe_{17}N_y$ and related compounds. It was suggested [70] that interstitial modification of $Nd_2Fe_{14}B$ using N results in an increase in T_c of 60 K, with a reduction in M_s and anisotropy field, B_a, but other studies have shown that nitrogenation leads directly to the decomposition [71,72]. Katter et al. [73] found that nitrogenation of Sm_2Co_{17} produced a significant decrease in T_c and M_s, while nearly doubling its anisotropy field.

3.1. Structure and magnetic properties of $R_2Fe_{17}N_{3-\delta}$ compounds

Without interstitial modification the intrinsic magnetic properties of the R_2Fe_{17} series render them useless as permanent magnet materials. As shown in Fig. 4, the Curie temperatures across the entire series of rare-earths are close to room temperature, the spontaneous magnetisation is low and the magnetocrystalline anisotropy is planar.

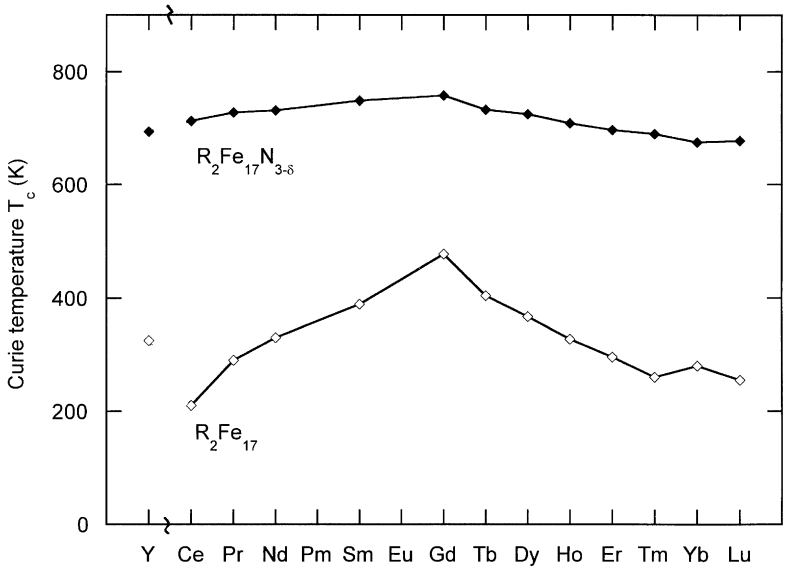

Fig. 4. Curie temperatures of R_2Fe_{17} and $R_2Fe_{17}N_{3-\delta}$ compounds, with and without nitrogen.

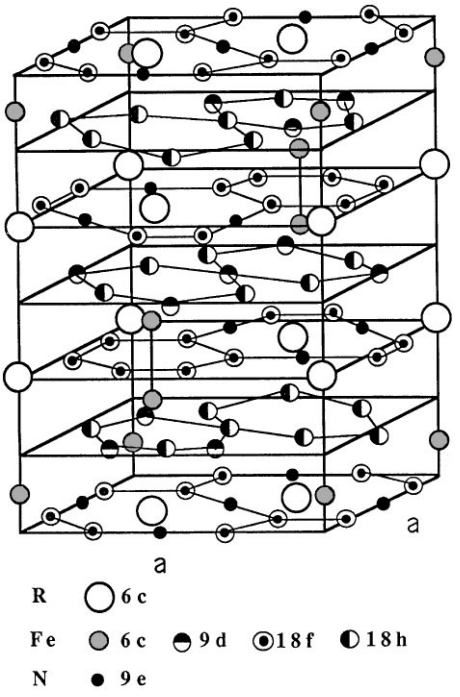

Fig. 5. Crystal structure of $Sm_2Fe_{17}N_3$.

The R_2Fe_{17} intermetallics crystallise in a rhombohedral Th_2Zn_{17}-type structure for light rare-earths (Fig. 5) and a hexagonal Th_2Ni_{17}-type structure for heavy rare-earths. The structures differ only in stacking sequence, and for R = Y, Gd and Tb both structure types can coexist. The low T_c and M_s for these compounds, in spite of their high Fe content, is attributed to the short Fe–Fe distance on the 6e (Th_2Zn_{17}) or 4f (Th_2Ni_{17}) 'dumbbell' sites, which leads to negative exchange and weakens the net positive exchange [74]. Self-consistent spin-polarised electronic structure calculations show that exchange is long range and positive on all sites, including the dumbbell sites [75]. Planar magnetocrystalline anisotropy for all but R = Tm is attributed to the dominant planar anisotropy of the Fe sublattice.

Upon exposure to N_2 gas at 1 bar, at temperatures between 620 and 770 K, nitrogen enters the lattice on 9e sites (Th_2Zn_{17}) or 6h sites (Th_2Ni_{17}), resulting in a volume expansion of 5–7%. This is associated with a dramatic enhancement of T_c (Fig. 4) and M_s across the entire series; for example in $Sm_2Fe_{17}N_{3-\delta}$, T_c increases from 389 to 749 K, and $\mu_0 M_s$ at 300 K increases from 1.0 T to 1.5 T. The parent compounds are weak ferromagnets, whereas nitrides and carbides exhibit nearly strong ferromagnetism [76]. Recently, Li and Morrish [77] measured the variation with temperature of magnetic hyperfine fields, using Mössbauer

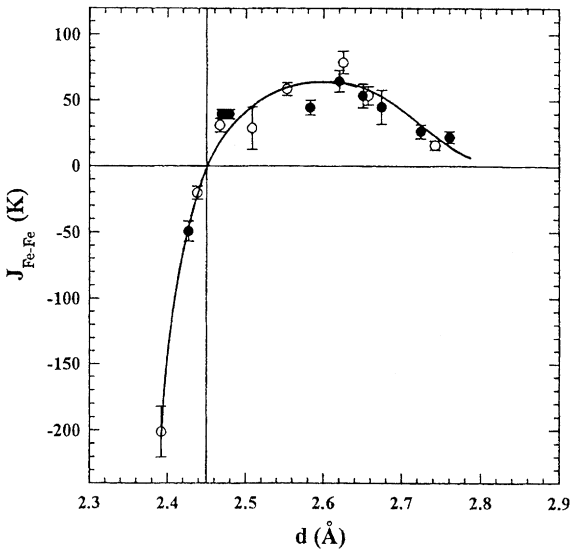

Fig. 6. Exchange interactions for Sm_2Fe_{17} (open circles) and $Sm_2Fe_{17}N_{3-\delta}$ (solid circles) as a function of Fe–Fe distance [77].

spectroscopy, from which the exchange integrals, J_{ij}, for each of the Fe–Fe pairs in Sm_2Fe_{17} and $Sm_2Fe_{17}N_3$ were calculated. The large negative value of -201 K for the 6c–6c (dumbbell) site in Sm_2Fe_{17} increases to -49 K upon nitrogenation, while a small negative value of -20 K for the 9d-18f pair becomes positive (39 K) and integrals for other pairs remain positive, in many cases increasing. This is rather direct microscopic evidence of the influence of nitrogenation on the Curie temperature. The nearest-neighbour exchange integrals are mainly determined by the Fe–Fe distance, which is increased by interstitial nitrogen, a plot of the data being reminiscent of the Bethe–Slater–Néel curve (Fig. 6). However, electronic structure calculations [75,78] show that the exchange interactions are long range. It is apparent from the calculations that J_{ij} is influenced by the environment, and is not only a function of bond length, according to the Bethe–Slater–Néel curve. There is a pronounced magnetovolume effect in R_2Fe_{17} compounds which is evident in both compression and expansion.

The increase in the room temperature spontaneous magnetisation can be attributed mostly to the enhancement of T_c, since M_s at 4 K increases by only about 10% on nitrogenation. The average moment per iron atom increases by 20%, but the increase in cell volume reduces the effect on the magnetisation [68].

The effects of nitrogen on the moments of the different sites have been studied by neutron diffraction [79] and Mössbauer studies [80] on the Y_2Fe_{17} compound, as well as by LSDA electronic structure calculation [39,81,82], results for which are shown in Table 2. The chemical effect of Fe–N hybridisation must again be distinguished from the effect of lattice dilation. The latter increases the moments on all the sites more or less uniformly, whereas the former has a tendency to reduce the moment of iron on sites with a nitrogen neighbour (18f and 18h in the Th_2Zn_{17} structure) while increasing the moment on the more distant sites (6c and 9d), as explained in Fig. 2 [43]. An advantage of the calculations is that the chemical effect can be

Table 2
Hyperfine fields and Fe site moments near 0 K measured using neutron diffraction and calculated for Y_2Fe_{17} (left columns) and $Y_2Fe_{17}N_{3-\delta}$ (right columns). (r) = rhombohedral structure, (h) = hexagonal structure

Fe site (h)/(r)	Hyperfine field (T) (h) [80]		Neutron diffraction (μ_B/atom) (r) [79]		Calculation (μ_B/atom) (h) [81]		Calculation (μ_B/atom) (r) [40]	
4f/6c	34.6	40.1	2.23	2.86	2.4	2.5	2.5	2.7
6g/9d	32.9	36.7	1.88	2.12	1.9	2.7	1.5	2.4
12j/18f	29.7	35.0	1.92	2.01	2.4	2.1	2.1	1.9
12k/18h	28.2	31.9	1.87	2.41	2.1	2.4	2.0	2.3
Average	31.4	35.9	1.98	2.35	2.2	2.4	2.0	2.2

separated from that of lattice expansion. Self-consistent calculations have been carried out for R_2Fe_{17} and $R_2Fe_{17}N_3$ in the atomic spheres approximation [39,81,83], and in the full-potential linear combination of atomic orbitals framework (FLMTO) [39,82], as well as non-self-consistent calculations using the orthogonalised linear combination of atomic orbitals (OLCAO) method [84].

The calculations reproduce the average moment per iron atom to within less than 10%, and show the existence of a small negative moment ($\sim -0.4\ \mu_B$) when R = Y, but little moment on nitrogen. Compared with neutron diffraction measurements in Table 2, there is a tendency to exaggerate the moment reduction due to hybridisation on the (18f and 18d) sites which have a nitrogen neighbour. The largest moment appears on the 6c site, which is farthest from nitrogen.

The average hyperfine constant changes little, from 15.7 T/μ_B to 15.3 T/μ_B on nitrogenation, but there is a range from 13–17 T/μ_B on the different sites, reflecting the relative importance of core polarisation, 4s and orbital terms [80].

It is only for R = Sm that nitrogenation changes the sign of the room temperature magnetocrystalline anisotropy. The transformation for $Sm_2Fe_{17}N_{3-\delta}$ is dramatic, with the planar anisotropy becoming strongly uniaxial, with $K_1 = 8.6\ MJ/m^3$, nearly twice that of $Nd_2Fe_{14}B$. This large increase is due to the electrostatic field created by the triangle of interstitial N atoms surrounding the Sm atoms (Fig. 5). The crystal field parameter A_2^0 is negative, and its value has been estimated as $-333\ Ka_0^{-2}$ or $-453\ Ka_0^{-2}$, according to whether or not J-mixing for Sm is included in the analysis [85]. Since the leading uniaxial anisotropy term can be written (in the absence of J-mixing) as

$$K_1^R = -\alpha_J \langle r_{4f}^2 \rangle A_2^0 \langle 3J_z^2 - J(J+1) \rangle \quad (1)$$

the sign of K_1 depends on whether the 4f orbitals are prolate or oblate, which is reflected in the sign if the Stevens coefficients α_J. Since α_J for Sm is 4.127×10^{-2}, the large magnetocrystalline anisotropy for $Sm_2Fe_{17}N_{3-\delta}$ is due to the combined effect of the prolate shape of the Sm 4f shell, the negative crystal field charge of nitrogen and the in-plane coordination of the interstitial 9e site [86].

None of the other rare-earths with a prolate 4f shell (Er, Tm, Yb) have a sufficiently strong crystal field interaction with nitrogen to overcome the planar anisotropy of the Fe sublattice ($K_1^{Fe} \approx -1.3\ MJ/m^3$).

A slight improvement of the magnetic properties of $Sm_2Fe_{17}N_{3-\delta}$ can be achieved by the substitution of Co for Fe. The anisotropy field reaches a peak of 23.7 T for $Sm_2(Fe_{1-x}Co_x)N_{3-\delta}$ at around $x = 0.2$, while M_s increases slightly [73]. The Curie temperature is increased to about 840 K. All rare-earth substitutions weaken the magnetocrystalline anisotropy. Substituting Nd increases M_s due to its higher atomic moment and it reduces the cost of the material. Simultaneously substituting Co for Fe makes up for the weakened uniaxial anisotropy. Katter et al. [87] reported intrinsic properties of $B_a = 14.8\ T$, $\mu_0 M_s = 1.57\ T$ and $T_c = 835\ K$ for $(Sm_{0.7}Nd_{0.3})_2(Fe_{0.8}Co_{0.2})_{17}N_{3-\delta}$. With 40% substitution of mischmetal for Sm an anisotropy field of 6.8 T, similar to that of $Nd_2Fe_{14}B$, could be maintained, while T_c was 150 K higher [88].

The combination of a large magnetocrystalline anisotropy, moderately high M_s and a T_c higher than that of $Nd_2Fe_{14}B$ immediately marked $Sm_2Fe_{17}N_{3-\delta}$ as a potential permanent magnet material. However, there have been considerable technical challenges in harnessing these intrinsic properties to produce magnets with useful coercivity, remanence and energy product, $(BH)_{max}$. The processing route is quite different from that used previously for any permanent magnets.

3.2. Processing of Sm–Fe–N materials

3.2.1. Production of Sm_2Fe_{17}

The precursor Sm_2Fe_{17} ingot material can be produced by arc-melting or induction melting, or by calciothermic reduction, in which Sm_2O_3, Fe and Ca powders are mixed, then heated at 1300 K to produce Sm_2Fe_{17} and CaO, which is washed away with water. Calciothermic reduction typically introduces a higher O impurity (>0.3 wt%), but recent improvements reduce the O content to less than 0.1 wt% [89]. When produced by casting, the Sm_2Fe_{17} phase forms by a peritectic reaction between the liquid Sm–Fe and γFe at 1550 K.

This makes it impossible to form single phase Sm_2Fe_{17} without a homogenisation treatment at $\sim$ 1200 K to remove $SmFe_3$ and αFe. The addition of 2 at% of a IVB, VB or VIB element reduces the amount of $SmFe_3$ phase and αFe [90], whilst adding 4–5 at% of Nb [91] or Ta [92] prevents primary crystallisation of Fe, although a paramagnetic Laves phase is formed. Recently Gebel et al. [93] showed that an addition of only 1 at% Zr suppressed formation of αFe, without adversely affecting magnetic properties. The elimination of $SmFe_3$ and αFe is essential as $SmFe_3$ decomposes to SmN and αFe during nitriding, and the presence of αFe provides nucleation sites for magnetisation reversal in small fields.

Other techniques which can be used to produce Sm_2Fe_{17} are mechanical alloying [94,95], in which elemental Sm and Fe are milled together in a high energy ball mill, and melt-spinning [96]. Homogenisation is not required since Sm_2Fe_{17} is formed either by crystallisation of an amorphous phase or by solid state reaction (on a scale of tens of nanometres) between amorphous Sm–Fe and αFe.

3.2.2. *Nitrogenation of Sm_2Fe_{17}*

Nitrogenation of Sm_2Fe_{17} powder is relatively simple; providing the size of powder particles is sufficiently small, exposure to N_2 gas at a pressure of $\sim$100 kPa, at temperatures in the range 620–770 K, leads to nearly complete nitrogenation within one to several hours according to the reaction

$$2Sm_2Fe_{17} + (3-\delta)N_2 \rightarrow 2Sm_2Fe_{17}N_{3-\delta}. \quad (2)$$

The ideal N content of 3 corresponds to complete filling of the 9e octahedral sites. However the value of δ is around 0.2, due to entropic considerations at elevated temperature. There may be a little nitrogen in the 18g tetragonal sites. Skomski [1] provides a nomograph giving the relationship between time for 90% nitrogenation, temperature and particle size. Nitrogenation does not occur within a reasonable time at temperatures below 620 K, and at temperatures in excess of 720 K disproportionation occurs according to the reaction

$$Sm_2Fe_{17}N_3 \rightarrow 2SmN + Fe_4N + 13Fe. \quad (3)$$

The change in free energy for disproportionation is more negative than for the nitrogenation reaction, and the formation of the nitride can be thought of an intermediate stage in the reaction between N_2 and Sm_2Fe_{17} to form the products shown in Eq. (3) [2]. Consequently, $Sm_2Fe_{17}N_{3-\delta}$ is metastable, but the disproportionation reaction does not proceed to any noticeable extent at temperatures below 720 K, due to the activation barrier for diffusion of Fe atoms [2]. The nitrogenation process is irreversible, so that once $Sm_2Fe_{17}N_{3-\delta}$ is formed, it is not possible to pump out the N atoms under vacuum on the same time scale as for nitrogenation.

A deeper understanding of the nitrogenation process is important, as the nitrogen content and the homogeneity of nitrogenation have a major influence on the magnetic properties of $Sm_2Fe_{17}N_{3-\delta}$. In particular, the presence of incompletely nitrided particles, with a soft magnetic Sm_2Fe_{17} core is highly detrimental to the coercivity. The mechanism of nitrogen diffusion has been considered in detail by Coey and Skomski [1,2,97], who proposed a mechanism of free diffusion in a gas–solid solution, and by Zhang and co-workers [98,99] who have put forward a model of trapping diffusion, or chemical reaction diffusion. Essentially, the difference between the two models is that in the free diffusion model, N atoms diffuse over 9e sites, and form a gas–solid solution, whilst in the trapping diffusion model, diffusion occurs via the energetically unfavourable 18g sites and an N atom falling onto a 9e site is chemically bound there and immobilised.

Many experimental data for $Sm_2Fe_{17}N_{3-\delta}$ favour free diffusion of N atoms in a gas–solid solution at typical nitrogenation temperatures (620–770 K). Intermediate lattice parameters have been observed [100], in association with intermediate Curie temperatures [73], and homogenisation treatments of partly nitrided grains lead to intermediate nitrogen concentrations [101]. Electron microscopy has revealed smooth nitrogen concentration profiles [102], and magnetic domain size distributions which can only be explained by intermediate anisotropy constants [103].

On the other hand, in situ observations of nitrogenation of Sm_2Fe_{17} using X-ray diffraction have

shown that a mixture of fully nitrided and non-nitrided material is present at all stages of the nitrogenation process [104] and there is a tendency to form core and shell structures in partly nitrogenated particles. NMR studies by Zhang et al. [99] on $Y_2Fe_{17}N_{3-\delta}$ powders have shown that powders with intermediate nitrogen contents contained two phases: a fully nitrided layer at the surface ($\delta = 0.2$) and the Y_2Fe_{17} parent phase in the interior, a configuration which was unchanged after annealing at 750 K for 12 h. It may be that $Y_2Fe_{17}N_{3-\delta}$ is more difficult to homogenise than $Sm_2Fe_{17}N_{3-\delta}$ [105]. The inability to desorb most N atoms under vacuum annealing is consistent with immobilisation of N atoms on 9e sites. In the free diffusion model, it is proposed that the existence of a surface layer and possibly the reassociation kinetics at the surface are responsible for this effect [2].

Regardless of the model, it is accepted that the temperature range for nitrogenation is well above the critical temperature below which a two phase region with a mixture of nitrogen-poor and nitrogen-rich areas would form due to the attractive interactions between N atoms. The fundamental difference is in the diffusion mechanism, not the phase constitution. Skomski and Wirth [106] recently found that trapping or immobilisation diffusion can produce smooth nitrogen profiles or step-like profiles, depending on the 9e and 18g site energies and the energy required to move from an 18g site to a 9e site. It is likely that the actual diffusion process may include aspects of both a trapping process and a free diffusion process.

In practice the presence of microcracks and microcrystalline grain boundaries provides easy diffusion paths, so that lower temperatures and shorter nitrogenation times are required than for homogeneous Sm_2Fe_{17} particles. The observations of a two-phase structure may be attributed to the different diffusion constants for short-circuit diffusion through defects and grain boundaries, and volume diffusion in the bulk [107].

Nitrogenation is also made easier by using nitrogen at high pressure [107,108] or by the use of hydrogen in a mixture with nitrogen, or in the form of NH_3 (which dissociates into N_2 and H_2 at typical nitriding temperatures). The effect of using NH_3 is to vastly increase the effective nitrogen pressure [2]. The equilibrium nitrogen concentration is increased, allowing N atoms to fill all of the 9e octahedral sites, along with some of the energetically unfavourable 18g sites, and N contents of up to 4 atoms per formula have been achieved [109]. Nitrogenation time to form $Sm_2Fe_{17}N_{3-\delta}$ are also reduced, possibly due to the ability of N to enter 18g sites, creating additional diffusion pathways. Nitrogen contents of more than 3 N/formula are detrimental to the magnetic properties, reducing K_1 sharply, and lowering T_c by about 10 K. Hydrogen pretreatment of powder has also been investigated by Fukuno and co-workers [110], who found that the nitrogenation process was significantly speeded due to the crack formation (akin to hydrogen decrepitation in $Nd_2Fe_{14}B$ [111]) which reduces diffusion distances. It may also lower the surface barrier for N to enter the particles, for example by removing any oxide layer and creating free surfaces.

3.2.3. Development of useful coercivity and energy product

The decomposition of $Sm_2Fe_{17}N_{3-\delta}$ at temperatures below the range in which sintering is possible means that the only way to produce magnets is to make high quality coercive $Sm_2Fe_{17}N_{3-\delta}$ powder, which is bonded either with a polymer or a metal such as Zn. Exceptions are the attempts to produce nearly full density magnets by shock compression [112,113] or by post-sintering nitrogenation [114] however, the properties achieved are no better than those of bonded magnets and mechanical stability is poor. Coercive powder can be produced in two ways: monocrystalline powder for anisotropic magnets can be made by carefully controlled milling of nitrided material, while there are several routes to produce polycrystalline high coercivity powder for isotropic magnets. Fig. 7 summarises these.

Usually it is vital to avoid the presence of the soft magnetic phases Sm_2Fe_{17} (due to incomplete nitrogenation) or αFe (due to nitriding for too long, allowing disproportionation). This necessitates a small particle size, which is typically achieved by ball milling or jet milling ingot material to an average particle size of 10–50 μm, with possible hydrogen pretreatment. Jakubowicz

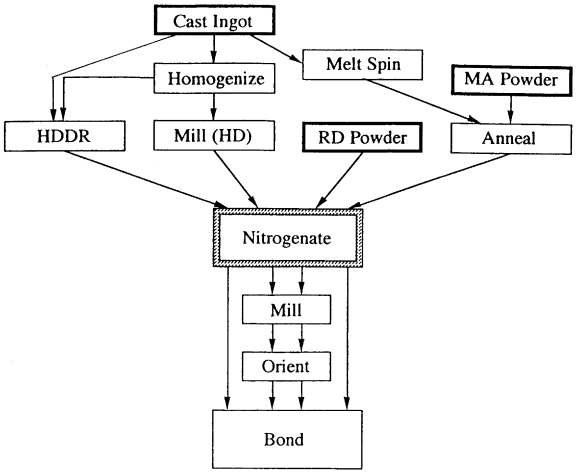

Fig. 7. Processing routes for $Sm_2Fe_{17}N_{3-\delta}$.

and Jurczyk [115] have recently reported that ball milling of Sm_2Fe_{17} in pyrazine ($C_4H_4N_2$) produced anisotropic $Sm_2Fe_{17}(C,N)_{3-\delta}$ powder with a coercivity of 0.55 MA/m. This process may have the potential for reducing the processing time and cost, although the coercivity is considerably smaller than that of the best powders produced by more conventional means. An interesting solid state process has been reported by Febri et al. [116], in which R_2Fe_{17} powder is mixed with sodium azide (NaN_3) powder and heated at 570–720 K, to produce fully nitrided $R_2Fe_{17}N_{3-\delta}$.

Coarse $Sm_2Fe_{17}N_{3-\delta}$ powder normally has low coercivity, as is typical for 3d–4f intermetallics, and further processing is required [117]. An exception is when ~ 8 at% V is substituted for Fe, producing a coercivity of 340 kA/m and initial magnetisation behaviour characteristic of a domain wall pinning mechanism [118]. The maximisation of coercivity in materials with a nucleation-type coercivity mechanism has been examined in detail with reference to $Nd_2Fe_{14}B$, by Kronmüller et al. [119]. An optimum particle size, smooth and undamaged particle surfaces, and isolation of misaligned single-crystal grains by a nonmagnetic phase are important to avoid easy nucleation of reversed domains. In $Sm_2Fe_{17}N_{3-\delta}$, the requirements are probably less stringent, due to the high anisotropy field (21 T compared to 8 T for $Nd_2Fe_{14}B$). The isolation of grains and smoothing of grain surfaces in sintered Nd–Fe–B magnets is achieved by adjusting the composition to provide a low melting point, paramagnetic Nd-rich intergranular phase, but the phase relations in Sm–Fe and metastability preclude such a technique in $Sm_2Fe_{17}N_{3-\delta}$ magnets. Therefore coercive monocrystalline powder can only be achieved by the careful control of processing parameters to optimise the quality of the powder.

The coercivity in $Sm_2Fe_{17}N_{3-\delta}$ powders has been found to increase with decreasing particle size, R_0, which implies a post-nitrogenation milling treatment [120]. Kobayashi et al. [121] explained an observed $1/R_0$ dependence of coercivity for particle sizes in the range 1–10 μm in terms of the isolation of larger centres for nucleation reversal in a small number of particles, using a statistical model. The single-domain particle size for $Sm_2Fe_{17}N_{3-\delta}$ is approximately 0.3 μm, but particles of size 1–3 μm exhibit behaviour consistent with single-domain reversal processes [117], which is explained by the fully magnetised state of the particles being quasi-stable. Useful coercivities of 550–800 kA/m are achieved by post-nitrogenation milling, thereby allowing the production of anisotropic polymer-bonded magnets with energy products in excess of 150 kJ/m^3 [122]. Zinc-bonding can be used to obtain coercivity in monocrystalline nitrided powders, with the effect of consuming αFe (by forming Zn_7Fe_3), isolating particles and smoothing their surfaces. However, the large amount of Zn required (15–25 wt%) reduces the remanence drastically and limits $(BH)_{max}$ to 80–90 kJ/m^3.

A further development of the post-nitrogenation milling process is the use of a surfactant [123]. Ball milling in a deoxygenated hexane solution containing a small amount of Aerosol OT produced coercivity of 1.13 MA/m, compared to 0.63 MA/m for a sample milled in hexane only. Alignment of the powders produced a remanence of 1.24 T with surfactant addition, increased from 1.0 T. Coating of the powders with a thin layer of Zn (< 1 wt%), using a photochemical deposition method, has been reported to greatly improve corrosion resistance and thermal stability. Remarkably stable powders were obtained after precoating with Cu, by reducing $CuCl_2$ during ball-milling, followed by Zn

Table 3
Coercivity, remanence and energy product for polycrystalline $Sm_2Fe_{17}N_{3-\delta}$ powders from different processes

Process	H_c (MA/m)	B_r (T)	$(BH)_{max}$ (kJ/m^3)	Ref.
Mechanical alloying	2.3	0.75	102	[95]
Rapid quenching	1.5	0.79*	102	[129]
HDDR	2.2	0.77	100	[130]

*$B_r > \frac{1}{2}M_s$ is due to the presence of α-Fe.

coating. Heating the Cu/Zn/$Sm_2Fe_{17}N_{3-\delta}$ powder in air at 320 K for ~ 24 h resulted in 10% flux loss, compared to 20% for Zn/$Sm_2Fe_{17}N_{3-\delta}$ and 30% for uncoated powder, and flux loss in an Ar atmosphere up to 620 K was negligible [124]. Using optimised milling conditions, $(BH)_{max}$ for the powder is 330 kJ/m^3 on average, and anisotropic epoxy-bonded magnets produced from Zn-coated powder had the highest $(BH)_{max}$ reported to date for a $Sm_2Fe_{17}N_{3-\delta}$ magnet, 176 kJ/m^3 [123,125].

Isotropic coercive powders have been produced by HDDR (hydrogen-disproportionation–desorption–recombination) [126], mechanical alloying, and melt spinning. As shown in Table 3, these techniques can yield very high coercivity, which is attributed to the nanoscale microstructure of the materials. Record coercivity of 3.5 MA/m was reported by Kuhrt et al. [127] for mechanically alloyed powder bonded under pressure with Zn at 720 K, due to the formation of a paramagnetic Zn_7Fe_3 intergranular phase. Melt spinning yields poor properties due to the formation of a $TbCu_7$-type phase in preference to the Th_2Zn_{17}-type phase [96], however Kleinschroth and Kronmüller [128] recently reported higher coercivity following heat treatment to remove the metastable $TbCu_7$-type phase prior to nitrogenation. A disadvantage of these three isotropic polycrystalline powders is the limited remanence of ~ 0.7 T, hence $(BH)_{max} \approx$ 100 kJ/m^3 (Table 3). Techniques available to thermomechanically densify and texture polycrystalline powders cannot be applied due to the disproportionation of $Sm_2Fe_{17}N_{3-\delta}$ at relatively low temperatures. Also, the production of anisotropic HDDR powder, which is possible in $Nd_2Fe_{14}B$-based material with an addition of 0.1 wt% Zr, has not yet been achieved for $Sm_2Fe_{17}N_{3-\delta}$ [129].

Improvements in the energy product of mechanically alloyed and melt-spun Sm–Fe–N materials have been made in nanocomposite (or exchange-spring) magnets, albeit at considerable cost in coercivity. Two-phase nanocomposites consist of a hard magnetic phase with large magnetocrystalline anisotropy, exchange coupled to a soft magnetic phase such as αFe, in a microstructure on a scale of 10 nm. They are isotropic but exhibit remanence in excess of $M_s/2$. Ding et al. first reported a mechanically alloyed $Sm_2Fe_{17}N_{3-\delta}$ + αFe (Sm_7Fe_{93}-N) nanocomposite with the remarkable remanence of 1.4 T in 1993 [130]. Useful coercivity (630–800 kA/m) was achieved for samples containing 9–11 at% Sm, with $(BH)_{max}$ for the powder estimated to be up to 160 kJ/m^3. A detailed characterisation of mechanically alloyed Sm_xFe_{100-x}-N nanocomposites was carried out by O'Donnell and Coey [131].

Yoneyama et al. [132,133] have overcome the problems associated with melt-spinning of Sm–Fe to produce commercially viable nanocomposite materials. The key innovation is the addition of 3 at% Zr, which promotes the formation of the almost fully amorphous ribbons during melt-spinning, thereby allowing better control of the microstructure. The Zr addition does not simply promote amorphisation, but also substitutes for Sm in the $TbCu_7$-type phase [134]. An increase in T_c of up to 800 K, well in excess of the accepted value of 740 K for $Sm_2Fe_{17}N_{2.8}$, may be due to an increase in the c/a ratio for the $TbCu_7$-type phase [135]. The best extrinsic properties were obtained for $(Sm_8Zr_3Fe_{89})_{85}N_{15}$ ribbons (containing ~ 20 vol% αFe), with $H_c = 713$ kA/m, $B_r = 0.91$ T and $(BH)_{max} = 104$ kJ/m^3. Substitution of 5 at% Co led to a further improvement, with $H_c = 740$ kA/m, $B_r = 0.95$ T and $(BH)_{max} = 126$ kJ/m^3, although T_c was reduced to 760 K. Epoxy-bonded magnets had an energy product of 80 kJ/m^3. These properties, along with excellent temperature and environmental stability [133] make these magnets superior to polymer-bonded MQ1 (Nd–Fe–B).

3.3. Future prospects for $Sm_2Fe_{17}N_{3-\delta}$ magnets

The main advantages of $Sm_2Fe_{17}N_{3-\delta}$ materials over $Nd_2Fe_{14}B$-based materials are an improved stability of the magnetic properties with respect to the elevated temperature and an ability to produce anisotropic bonded magnets. It is on these bases that $Sm_2Fe_{17}N_{3-\delta}$ magnets will enter the market. Commercial production of polymer-bonded anisotropic fine particle magnets has recently been announced by both Sumitomo Mining and Metallurgy and Hitachi. When reporting properties of (Sm,Zr)Fe_7 + αFe nanocomposite bonded magnets in 1996 [133], TDK Corporation proclaimed the 'opening of a new age of isotropic bonded magnets'. Polymer bonding appears to be the only viable production route, due to the restrictions on processing temperature imposed by metastability. The prospect is that Sm–Fe–N will now, ten years after its discovery, capture a segment of the fast-growing bonded magnet market.

4. Other 3d–4f nitrides

4.1. $ThMn_{12}$-type

The tetragonal $ThMn_{12}$-type intermetallics with a general formula $R(Fe_{12-x}M_x)$ are stabilised by elements M = V, Mo, Ti. Unlike the R_2Fe_{17} series, the Fe sublattice has uniaxial magnetocrystalline anisotropy, and for M = Ti, all compounds except R = Pr and Tb exhibit uniaxial anisotropy, due to the dominance of Fe sublattice. A_2^0 is small and negative, so compounds with R = Sm have the best hard magnetic properties. Upon nitrogenation, the Fe sublattice anisotropy remains uniaxial, but the rare-earth anisotropy is dramatically changed by the rare-earth atoms having two nitrogen nearest-neighbours located along the *c*-axis. This produces a strongly positive $A_2^0 \approx 300\ \mathrm{Ka}_0^{-2}$. For R = Sm, Er and Tm, this results in planar anisotropy, while for all other rare-earths, there should be uniaxial anisotropy. The size of the anisotropy fields measured for $RFe_{12-x}M_xN_y$ depends to some extent on the value of *x*, and the nitrogen content, so that there is considerable scatter in the published values (see the tables in Ref. [68]), however they are consistently high, in the range 7–12 T for R = Nd, Pr, Tb and Dy.

Nitrogen locates on similar octahedral interstitial sites to those in Sm_2Fe_{17}, with a theoretical maximum concentration of 1 atom per formula unit. Volume expansions of 2–4% have been measured, lower than those for $R_2Fe_{17}N_x$, but the Curie temperatures of Ti-stabilised compounds are similar (740 K for $Sm(Fe_{11}Ti)N_y$). Mo-stabilised compounds have generally lower Curie temperatures, in the range 480–700 K.

A low R : Fe ratio, and good properties for the more abundant rare-earths Nd and Pr make the $R(Fe_{12-x}M_x)$Ny compounds attractive as permanent magnet materials. The most interesting are $Nd(Fe_{12-x}M_x)N_y$ (M = Mo, V, Ti) and $Pr(Fe_{12-x}Mo_x)$Ny, for which typical magnetic properties are shown in Table 4. Yang et al. [139] have recently reported moderately large energy products ($\sim 135\ \mathrm{kJ/m^3}$) for anisotropic fine powder magnets made from $Nd(Fe_{10.5}V_{1.5})N_y$ with $y \approx 1$, although $(BH)_{max}$ is limited by low coercivity (330 kA/m). A number of reports have been made of the coercive powder produced by mechanical alloying, with coercivities of 600–700 kA/m reported for $NdFe_{12-x}V_xN_y$ [140,141]. This is rather low, even when compared with the mechanically alloyed $Nd_2Fe_{14}B$ [142], for which the anisotropy field is similar. Unless properties comparable to those for $Sm_2Fe_{17}N_{3-\delta}$ are achieved for anisotropic fine powder, it is likely that $ThMn_{12}$-type materials will remain of academic interest.

4.2. $R_3(Fe, M)_{29}$-type

The latest series of rare-earth transition metal nitrides are based on the monoclinic $R_3Fe_{29-x}M_x$ structure (M = Ti, V, Cr, Mo, Mn) [143,144], previously identified by Collocott et al. in 1992 as $R_2(Fe,Ti)_{19}$ [145]. Like the 2 : 17 and 1 : 12 type compounds, the 3 : 29 series represents a modification of the $CaCu_5$-type structure, in which a fraction of the R atoms are replaced by transition metal dumbbell pairs. Table 5 shows the intrinsic magnetic properties of some representative examples of the series, along with the properties measured after nitrogenation. There are two large interstitial

Table 4
Room temperature intrinsic magnetic properties of selected $RFe_{12-x}M_x$ compounds before and after nitrogenation

	x	T_c (K)	σ_s ($JT^{-1}kg^{-1}$)	B_a (T)	Ref.
$NdFe_{12-x}V_x$	2.0	583	109	1.8	[136]
$NdFe_{12-x}V_xN_y$	2.0	743	113	7.5	[136]
$NdFe_{12-x}Mo_x$	1.25	470	121	0.4	[137]
$NdFe_{12-x}Mo_xN_y$	1.25	650	120	9.4	[137]
$NdFe_{12-x}Ti_x$	1.0	547	141	2.0	[68]
$NdFe_{12-x}Ti_xN_y$	1.0	640	144	8.0	[68]
$PrFe_{12-x}Mo_x$	1.5	455	112	planar	[138]
$PrFe_{12-x}Mo_xN_y$	1.5	740	121	11	[138]

Table 5
Intrinsic magnetic properties of the selected $R_3Fe_{29-x}M_x$ compounds and their nitrides at room temperature

	x	T_c (K)	σ_s ($JT^{-1}kg^{-1}$)	B_a (T)	Ref.
$Sm_3Fe_{29-x}V_x$	2.3	502	92	4.3	[147]
$Sm_3Fe_{29-x}V_xN_4$	2.3	683	136	6.7	[147]
$Sm_3Fe_{29-x}Ti_x$	1.9	486	119	3.4	[143]
$Sm_3Fe_{29-x}Ti_xN_4$	1.9	750	140	12.8	[143]
$Sm_3Fe_{29-x}Cr_x$	4.3	437	68	–	[149]
$Sm_3Fe_{29-x}Cr_xN_{5.7}$	4.3	713	102	$\geqslant 6$	[149]
$Nd_3Fe_{29-x}Ti_x$	1.1	396	130	7.7	[141]
$Nd_3Fe_{29-x}Ti_xN_{4.7}$	1.1	725	164	8.1	[141]
$Pr_3Fe_{29-x}Ti_x$	1.4	373	127	4.0	[141]
$Pr_3Fe_{29-x}Ti_xN_{5.4}$	1.4	700	170	7.5	[141]

octahedral sites on which N atoms locate, leading to a maximum N concentration of 4 atoms per formula unit, which leads to a volume expansion of $\sim 6\%$. Hu et al. [146] have performed neutron diffraction study on $Nd_3(Fe,Ti)_{29}N_4$, showing that most Fe–Fe bond lengths increase, while some decrease. The net effect is clearly a more positive exchange, given the increase in T_c upon nitrogenation. The saturation magnetisation also increases, and is comparable to that of $Sm_2Fe_{17}N_{3-\delta}$ for (R, M) = (Nd, Ti) and (Pr, Ti) (see Table 5).

There is considerable uncertainty in the literature about the anisotropy fields of 3 : 29 compounds. Cadogan et al. [144] reported that room temperature anisotropy fields for $Sm_3(Fe, M)_{29}N_4$ are in the range 10–13 T, increased from ~ 3 T for the non-nitrided compound, while for $Nd_3(Fe,M)_{29}N_4$, B_a is ~ 8 T, with little increase upon nitrogenation. Han et al. [147] reported an anisotropy field of only 6.7 T for $Sm_3(Fe_{26.7}V_{2.3})N_4$, whilst Koyama et al. [149] reported a value of > 7 T for $Sm_3(Fe_{26.3}V_{2.7})N_5$. The magnetocrystalline anisotropy of these compounds is complicated by their monoclinic structure. Wirth et al. [150] point out that two anisotropy constants are required to describe the magnetocrystalline anisotropy energy in the lowest order, and they present details of a method to determine the anisotropy constants by fitting experimental demagnetisation curves. The description of the magnetocrystalline anisotropy energy is made using a superposition of contributions from the 2 : 17 and 1 : 12 building blocks forming the 3 : 29 structure.

In terms of producing permanent magnet materials, $Sm_3(Fe,V)_{29}N_4$ is the most interesting of the 3 : 29 compounds, having an anisotropy field and Curie temperature higher than those of $Nd_2Fe_{14}B$ and similar saturation magnetisation at room temperature. Coercive powders, presumably nanocrystalline, have been produced by high intensity ball milling, with $H_c = 600$ kA/m, $B_r = 0.94$ T and $(BH)_{max} = 108$ kJ/m^3 [146]. The rather high remanence can be attributed to the presence of αFe, but there are no reports of coercive monocrystalline powder.

5. Conclusions

Interstitial modification of 3d metals and 3d–4f intermetallic compounds by nitrogenation leads to

a dilation of the crystal lattice and changes in the electronic structure which produce significant changes in the intrinsic magnetic properties of iron-based materials. They tend to become strong ferromagnets, with increased magnetisation and Curie temperature. There is no consensus in favour of the *average* iron moments in excess of the Slater–Pauling extrapolation, although certain sites with a low 3d electron density may have moments as high as 3 μ_B. The interstitial nitrogen induces anisotropy in both the iron and rare-earth sublattices, but it is particularly effective in the latter case because it tends to occupy octahedral sites adjacent to the rare-earth. A_2^0 may be positive for an axial, dumbbell arrangement of the nitrogen (1 : 12 structure) or negative for an in-plane triangle (2 : 17 structure). The rare-earth crystal field is at the origin of the excellent hard magnetic properties obtained by nitrogenation of $Sm_2Fe_{17}N_{3-\delta}$ which are now leading to its development as a commercial permanent magnet material. On the contrary, in soft ferromagnets, the anisotropy associated with nitrogen in usually unwelcome, hence the emphasis on nanocrystalline alloys with low nitrogen content, where the anisotropy may be averaged out over the exchange length.

References

[1] R. Skomski in: J.M.D. Coey (Ed.), Rare-earth – Iron Permanent Magnets, Clarendon Press, Oxford, 1996 (Chapter 4).
[2] J.M.D. Coey, J. Magn. Magn. Mater. 159 (1996) 80.
[3] K.H. Jack, Proc. Roy. Soc. A 208 (1951) 200, 216.
[4] J. Foct, J. Phys. 35 (1974) C6-487.
[5] M.A. Rusak, C.V. Jahnes, E. Klokholm, J.W. Lee, M.E. Re, B.C. Webb, J. Magn. Magn. Mater. 104–107 (1992) 1853.
[6] H. Takahashi, H. Shoji, M Takahashi, J. Magn. Magn. Mater. 174 (1997) 57.
[7] S. Wang, M.H. Kryder, J. Appl. Phys. 67 (1990) 5134.
[8] T. Ohgai, R. Shimona, H. Saito, Y. Hayashi, Mater. Trans. Jpn. Inst. Met. 38 (1997) 503.
[9] N. Terada, Y. Hoshi, S. Yamanaka, IEEE Trans. Magn. 20 (1984) 1451.
[10] M.H. Kryder, J.A. Bain, Min Xiao, Proceedings of the Third International Symposium on Physics of Magnetic Materials, Seoul, 1995, p. 457.
[11] B. Ma, F.L. Wei, X.X. Lu, C.T. Xiao, Z. Yang, Mater. Sci. Eng. B 57 (1999) 97.
[12] P.H. Zheng, J.A. Bain, M.H. Kryder, IEEE Trans. Magn. 32 (1996) 4541.
[13] L. Varga, H. Jiang, T.J. Klemer, W.D. Doyle, IEEE Trans. Magn. 34 (1998) 1441.
[14] D.L. Peng, K. Sumiyana, K. Suzuki, J. Alloys Compounds 255 (1997) 50.
[15] S. Wang, K.E. Obermyer, M.H. Kryder, IEEE Trans. Magn. 27 (1991) 4879.
[16] W.P. Jayasekara, J.A. Bain, M.H. Kryder, IEEE Trans. Magn. 34 (1998) 1438.
[17] W. Maass, H. Rohrmann, IEEE Trans. Magn. 34 (1998) 1435.
[18] K. Sin, C.-T. Wang, S.X. Wang, B.M. Clemens, J. Appl. Phys. 81 (1997) 4507.
[19] M.Q. Huang, W.E. Wallace, S. Simizu, S.G. Sankar, J. Magn. Magn. Mater. 135 (1994) 226.
[20] Y. Sugita, H. Takahashi, M. Komuro, K. Mitsuoka, A. Sakuma, J. Appl. Phys. 76 (1994) 6637.
[21] M.A. Brewer, C.J. Escher, K.M. Krishnan, T. Kobayashi, A. Nakanishi, J. Appl. Phys. 81 (1997) 4128.
[22] S. Okamoto, O. Kitakami, Y. Shimoda, J. Appl. Phys. 79 (1996) 1678.
[23] H. Shinno, K. Saito, Surf. Coat. Technol. 103–104 (1998) 129.
[24] A. Boettger, M.L. van Genderen, K. Han, E.J. Mittemeijer, J. Phys. IV 7 (1997) C5-257.
[25] H. Tanaka, S. Nagakura, Y. Nakamura, Y. Hirotsu, Acta Mater. 45 (1997) 1401.
[26] J.M.D. Coey, K. O'Donnell, Q. Qi, E. Touchais, K.H. Jack, J. Phys.: Condens. Matter 6 (1994) L23.
[27] P. Bezdicka, A. Klarikova, I. Paseka, K. Zaveta, J. Alloys Compounds 274 (1998) 10.
[28] M. Komura, H. Hoshiya, M. Mitsuoka, Y. Kozono, M. Hanazono, Y. Sugita, J. Appl. Phys. 67 (1990) 5126.
[29] Y. Sugita, M. Mitsuoka, M. Komura, H. Hoshiya, Y. Kozono, M. Hanazono, J. Appl. Phys. 70 (1991) 597.
[30] Y. Sugita, H. Takahashi, M. Komuro, M. Igarashi, R. Imura, T. Kambe, J. Appl. Phys. 79 (1996) 5576.
[31] K. Nakajima, S. Okamoto, J. Appl. Phys. 65 (1989) 4357.
[32] S. Okamoto, O. Kitakami, Y. Shimada, J. Appl. Phys. 79 (1996) 5250.
[33] Z.Y. Yao, H. Jiang, Z.K. Liu, D.D. Huang, F.G. Qin, S.C. Zhu, Y.X. Sun, J. Magn. Magn. Mater. 177–181 (1998) 1291.
[34] T.K. Kim, M. Takahashi, Appl. Phys. Lett. 20 (1972) 492.
[35] S. Okamoto, O. Kitakami, Y. Shimada, J. Appl. Phys. 85 (1999) 4952.
[36] J.M.D. Coey, J. Appl. Phys. 76 (1994) 6632.
[37] A. Sakuma, J. Appl. Phys. 79 (1996) 5570.
[38] R. Coehoorn, G.H.O. Daalderop, H.J.F. Jansen, Phys. Rev. B 48 (1993) 3830.
[39] H. Tanaka, H. Harima, T. Yamamoto, H. Katayama-Yoshida, Y. Nakata, Y. Hirotsu, J. Magn. Magn. Mater. 177–181 (1998) 1468.
[40] S. Asano, M. Yamaguchi, Physica B 237–238 (1997) 541.
[41] H. Nakajima, Y. Ohashi, K. Shiiji, J. Magn. Magn. Mater. 167 (1997) 259.
[42] Q. Qi, K. O'Donnell, E. Touchais, J.M.D. Coey, Hyperfine Interactions 94 (1994) 2067.

[43] J. Kanamori, Prog. Theor. Phys. Supp. 101 (1990) 1.
[44] Y.D. Zhang, J.I. Budnick, W.A. Hines, M.Q. Huang, W.E. Wallace, Phys. Rev. B 54 (1996) 51.
[45] T. Moriya, Y. Sumimoto, H. Ino, F.E. Fujita, Y. Maeda, J. Phys. Soc. Japan 35 (1973) 1378.
[46] K. Nakajima, S. Okamoto, T. Okada, J. Appl. Phys. 65 (1989) 4357.
[47] R.M. Metzger, X. Bao, M. Carbucicchio, J. Appl. Phys. 76 (1994) 6626.
[48] T. Weber, L. de Wit, F.W. Saris, P. Schaaf, Thin Solid Films 279 (1996) 216.
[49] K.H. Jack, J. Appl. Phys. 76 (1994) 6620.
[50] H.Y. Wang, E.Y. Jiang, J. Phys.: Condens. Matter 9 (1997) 2739.
[51] M. Takahashi, H. Takahashi, H. Nashi, H. Shoji, T. Wakiyama, M. Kuwubara, J. Appl. Phys. 79 (1996) 5564.
[52] A.R. Williams, V.L. Moruzzi, A.P. Malozemoff, K. Tekura, IEEE Trans. Magn. 22 (1983) 1983.
[53] T. Osaka, M. Takai, K. Hayashi, Y. Sogawa, K. Ohasi, Y. Yasue, M. Saito, K. Yamada, IEEE Trans. Magn. 34 (1998) 1432.
[54] I.M.L. Billas, J.A. Becker, A. Chatelain, W.A. Deheer, Phys. Rev. Lett. 71 (1994) 4067.
[55] L. Del Bianco, C. Ballesteros, J.M. Rojo, A. Hernando, Phys. Rev. Lett. 81 (1998) 4500.
[56] K. O'Donnell, X.L. Rao, G. Laird, J.M.D. Coey, Phys. Stat. Sol. (a) 153 (1996) 223.
[57] B.C. Frazer, Phys. Rev. 112 (1958) 751.
[58] C.A. Kuhnen, R.S. de Figuerdo, V. Drago, E.Z. da Silva, J. Magn. Magn. Mater. 111 (1992) 95.
[59] P. Mohn, S.F. Matar, J. Magn. Magn. Mater. 191 (1999) 234.
[60] P. Mohn, K. Schwarz, S. Matar, G Demazeau, Phys. Rev. B 45 (1992) 4000.
[61] D. Fruchart, D. Givord, P. Convert, P. l'Héritier, J.P. Senateur, J. Phys. F 9 (1979) 2431.
[62] S. Matar, B. Siberchicot, M. Pénicaud, G. Demazeau, J. Phys. I 2 (1992) 1819.
[63] T. Hinomura, S. Nasu, Hyperfine Interactions 111 (1998) 221.
[64] L. Rissanen, M. Neubauer, K.P. Lieb, P. Schaaf, J. Alloys Compounds 274 (1998) 74.
[65] L. Risannen, M. Neubauer, K.P. Lieb, P. Schaaf, J. Alloys Compounds 274 (1998) 74.
[66] G. Herzer, in Handbook of Magnetic Materials (ed. K.H.J. Buschow), North-Holland, Amsterdam, 1997, vol. 10, p 417.
[67] J.M.D. Coey, Hong Sun, J. Magn. Magn. Mater. 87 (1990) L251.
[68] H. Fujii, H. Sun, in: K.H.J. Buschow (Ed.), Handbook of Magnetic Materials, Vol. 9, North-Holland, Amsterdam, 1995, p. 303.
[69] K. Kobayashi, Proceedings Thirteenth International Workshop on Rare-Earth Magnets and Their Applications, University of Birmingham, 1994, p. 717.
[70] Y.C. Yang, X.D. Zhang, L.S. Kong, Q. Pan, Y.T. Hou, S. Huang, L. Yang, S.L. Ge, J. Less-Common Met. 170 (1991) 37.
[71] C. Önneby, T. DeBroy, S. Seetharaman, J. Magn. Magn. Mater. 127 (1993) 30.
[72] T.P. Blach, E. MacA. Gray, J. Magn. Magn. Mater. 177–181 (1998) 985.
[73] M. Katter, J. Wecker, C. Kuhrt, L. Schultz, R. Grössinger, J. Magn. Magn. Mater. 114 (1992) 35.
[74] D. Givord, R. Lemaire, IEEE Trans. Magn. 10 (1974) 109.
[75] R.F. Sabiryanov, S.S. Jaswal, Phys. Rev. B 57 (1998) 7767.
[76] X.-L. Rao, R. Skomski, Q.-N. Qi, J.M.D. Coey, Phys. Stat. Sol. (b) 186 (1994) K23.
[77] Z.W. Li, A.H. Morrish, Phys. Rev. B 55 (1997) 3670.
[78] R.F. Sabiryanov, S.S. Jaswal, Phys. Rev. Lett. 79 (1997) 155.
[79] H. Fujii, K. Koyama, K. Tatami, S. Mitsudo, M. Motokawa, T. Kajitani, Y. Morii, P.C. Canfield, Physica B 237–238 (1997) 534.
[80] Q.-N. Qi, H. Sun, R. Skomski, J.M.D. Coey, Phys. Rev. B 45 (1992) 12278.
[81] T. Beuerle, M. Fähnle, Phys. Stat. Sol. (b) 174 (1992) 257.
[82] P. Ubele, K. Hummler, M. Fähnle, Phys. Rev. B 53 (1996) 3296.
[83] S.S. Jaswal, W.B. Yelon, G.C. Hadjipanayis, Y.Z. Wang, D.J. Sellmyer, Phys. Rev. Lett. 67 (1991) 644.
[84] Y.-P. Li, H.-S. Li, J.M.D. Coey, Phys. Stat. Sol. (b) 166 (1991) K107.
[85] M. Kuz'min, J.M.D. Coey, Phys. Rev. B 50 (1994) 12553.
[86] R. Skomski, M. Kuz'min, J.M.D. Coey, J. Appl. Phys. 73 (1993) 6934.
[87] M. Katter, J. Wecker, C. Kuhrt, L. Schultz, X.C. Kou, R. Grossinger, J. Magn. Magn. Mater. 111 (1992) 293.
[88] M.Q. Huang, Y. Zheng, K. Miller, J.M. Elbicki, W.E. Wallace, R. Obermeyer, J. Magn. Magn. Mater. 102 (1991) 91.
[89] H. Kawamoto, H. Ishikaza, S. Yasuda, K. Takeya, T. Ishikawa, K. Ohmori, Digests of the 21st Annual Conference on Magnetics in Japan, 1997, p. 371.
[90] X. Chen, Z. Altounian, J. Appl. Phys. 75 (1994) 6012.
[91] A.E. Platts, I.R. Harris, J.M.D. Coey, J. Alloys Compounds 185 (1992) 251.
[92] B. Saje, A.E. Platts, S. Kobe Besenicar, I.R. Harris, D. Kolar, IEEE Trans. Magn. 30 (1994) 690.
[93] B. Gebel, M. Kubis, K.-H. Müller, J. Magn. Magn. Mater. 174 (1997) L1.
[94] K. Schnitzke, L. Schultz, J. Wecker, M. Katter, Appl. Phys. Lett. 57 (1990) 2853.
[95] J. Ding, P.G. McCormick, R. Street, J. Alloys Compounds 189 (1992) 83.
[96] M. Katter, J. Wecker, L. Schultz, J. Appl. Phys. 70 (1991) 3188.
[97] R. Skomski, J.M.D. Coey, J. Appl. Phys. 73 (1993) 7602.
[98] Y.D. Zhang, J.I. Budnick, W.A. Hines, J. Appl. Phys. 79 (1996) 4596.
[99] Y.D. Zhang, J.I. Budnick, W.A. Hines, N.X. Shen, J.M. Gronek, J. Phys.: Condens. Matter 9 (1997) 1201.
[100] S. Brennan, R. Skomski, Q.-N. Qi, J.M.D. Coey 140–144 (1995) 999.
[101] T. Mukai, T. Fujimoto, J. Magn. Magn. Mater. 103 (1992) 165.

[102] R. Skomski, K. Kobayashi, S. Brennan, J.M.D. Coey, J. Magn. Magn. Mater. 140–144 (1995) 1079.
[103] K.-H. Müller, P.A.P. Wendhausen, D. Eckert, A. Handstein, Proceedings of the Seventh International Symposium on Anisotropy and Coercivity in RE-TM Alloys, Canberra, 1992, p. 34.
[104] A. Teresiak, B. Gebel, A. Handstein, N. Mattern, H. Klose, K.-H. Müller, Fres. J. Anal. Chem. 361 (1998) 674.
[105] S. Brennan, Ph.D. Thesis, Trinity College Dublin, 1995.
[106] R. Skomski, S. Wirth, J. Appl. Phys. 83 (1998) 6896.
[107] H. Fujii, K. Tatami, K. Koyama, J. Alloys Compounds 236 (1996) 156.
[108] O. Isnard, S. Miraglia, J.L. Soubeyroux, D. Fruchart, J. Alloys Compounds 190 (1992) 129.
[109] R. Skomski, S. Brennan, J.M.D. Coey, Phys. Stat. Sol. (a) 139 (1993) K11.
[110] A. Fukuno, C. Ishizaka, T. Yoneyama, Proceedings of the Twelfth International Workshop on Rare-Earth Magnets and Their Applications, Canberra, 1992, p. 60.
[111] P.J. McGuiness, I.R. Harris, E. Rozendaal, J. Ormerod, M. Ward, J. Mater. Sci. 21 (1986) 4107.
[112] B.-P. Hu, X.-L. Rao, J.M. Xu, G.-C. Liu, Y.-Z. Wang, X.-L. Dong, D.-X. Zhang, M. Cai, J. Appl. Phys. 74 (1993) 489.
[113] T. Mashimo, S. Tashiro, S. Hirosawa, K. Makita, J. Appl. Phys. 80 (1996) 356.
[114] X. Chen, Z. Altounian, J.O. Ström-Olsen, J. Appl. Phys. 81 (1997) 4557.
[115] J. Jakubowicz, M. Jurczyk, J. Alloys Compounds 266 (1998) 318.
[116] M. Febri, P. Ezekwenna, P. Chaudouët, Ph. l'Héritier, J.C. Joubert, J. Magn. Magn. Mater. 157–158 (1996) 103.
[117] K. Kobayashi, T. Iriyama, T. Yamaguchi, H. Kato, Y. Nakagawa, J. Alloys Compounds 193 (1993) 235.
[118] S. Suzuki, S. Suzuki, M. Kawasaki, J. Appl. Phys. 76 (1994) 6708.
[119] H. Kronmüller, K.-D. Durst, M. Sagawa, J. Magn. Magn. Mater. 74 (1988) 291.
[120] A. Fukuno, C. Ishizaka, T. Yoneyama, Proc. Twelfth International Workshop on Rare-Earth Magnets and their Applications, Canberra, 1992, p. 60.
[121] K. Kobayashi, R. Skomski, J.M.D. Coey, J. Alloys Compounds 222 (1995) 1.
[122] S. Suzuki, T. Miura, M. Kawasaki, IEEE Trans. Magn. 29 (1993) 2815.
[123] K. Machida, H. Izumi, A. Shiomi, M. Iguchi, G. Adachi, Proceedings of the Fourteenth International Workshop on Rare-Earth Magnets and Their Applications, World Scientific, Singapore, 1996, p. 203.
[124] K. Noguchi, K. Machida, M. Nishimura, G. Adachi, Proceedings of the Fifteenth International Workshop on Rare-Earth Magnets and Their Applications, Werkstoff-Informationgesellschaft, Frankfurt, 1998, p. 915.
[125] H. Izumi, K. Machida, A. Shiomi, M. Iguchi, K. Noguchi, G.Y. Adachi, Chem. Mater. 9 (1997) 2759.
[126] H. Nakamura, S. Sugimoto, M. Okada, M. Homma, Mater. Chem. Phys. 32 (1992) 280.
[127] Ch. Kuhrt, K. O'Donnell, M. Katter, J. Wecker, K. Schnitzke, L. Schultz, Appl. Phys. Lett. 60 (1992) 3316.
[128] I. Kleinschroth, H. Kronmüller, Proceedings of the Ninth International Symposium on Magnetic Anisotropy and Coercivity in Rare-Earth Transition Metal Alloys, World Scientific, Singapore, 1996, p. 97.
[129] N.M. Dempsey, Ph. D. Thesis, Trinity College Dublin, 1998.
[130] J. Ding, P.G. McCormick, R. Street, J. Magn. Magn. Mater. 124 (1993) L1.
[131] K. O'Donnell, J.M.D. Coey, J. Appl. Phys. 81 (1997) 6310.
[132] T. Yoneyama, T. Yamamoto, T. Hikada, Appl. Phys. Lett. 67 (1995) 3197.
[133] T. Yamamoto, T. Hikada, T. Yoneyama, H. Nishio, A. Fukuno, Proceedings of the Fourteenth International Workshop on Rare-Earth Magnets and Their Applications, World Scientific, Singapore, 1996, p. 121.
[134] T. Hidaka, T. Yamamoto, H. Nakamura, A. Fukuno, J. Appl. Phys. 83 (1998) 6917.
[135] S. Sakaruda, A. Tsutai, T. Hirai, Y. Yanagida, M. Sahashi, S. Abe, T. Kaneko, J. Appl. Phys. 79 (1996) 4611.
[136] Y.-Z. Wang, G.C. Hadjipanayis, A. Kim, D.J. Sellmyer, W.B. Yelon, J. Magn. Magn. Mater. 104–107 (1992) 1132.
[137] Y.-C. Yang, Q. Pan, X.-D. Zhang, M.-H. Zhang, C.-L. Yang, Y. Li, S.-L. Ge, B.-F. Zhang, J. Appl. Phys. 74 (1993) 4066.
[138] Y.-Z. Wang, B.-P. Hu, X.-L. Rao, G.-C. Liu, L. Yin, W.-Y. Lai, W. Gong, G.-C. Hadjipanayis, J. Appl. Phys. 73 (1993) 6251.
[139] J. Yang, B. Cui, B. Cheng, W. Mao, Y.-C. Yang, S. Ge, J. Phys. D: Appl. Phys. 31 (1998) 282.
[140] L. Schultz, K. Schnitzke, J. Wecker, M. Katter, C. Kuhrt, J. Appl. Phys. 70 (1991) 6339.
[141] J. Yang, M. Qu, Z. Altounian, J. Appl. Phys. 79 (1996) 5519.
[142] L. Schultz, J. Wecker, Mater. Sci. Eng. 99 (1988) 127.
[143] F.-M. Yang, B. Nasunjilegal, J.-L. Wang, H.-Y. Pan, W.-D. Qing, R.-W. Zhao, B.-P. Hu, Y.-Z. Wang, G.-C. Liu, H.-S. Li, J.M. Cadogan, J. Appl. Phys. 76 (1994) 1971.
[144] J.M. Cadogan, H.-S. Li, A. Margarian, J.B. Dunlop, D.H. Ryan, S.J. Collocott, R.L. Davis, J. Appl. Phys. 76 (1994) 6138.
[145] S.J. Collocott, R.K. Day, J.B. Dunlop, R.L. Davis, Proceedings of the Seventh International Symposium on Magnetic Anisotropy and Coercivity in RE-TM Alloys, Canberra, 1992, p. 437.
[146] Z. Hu, W.B. Yelon, O. Kalogirou, V. Psycharis, J. Appl. Phys. 80 (1996) 2955.
[147] X.-F. Han, F.-M. Yang, Q.-S. Li, M.-C. Zhang, S.-Z. Zhou, J. Phys.: Condens. Matter 10 (1998) 151.
[149] K. Koyama, H. Fujii, S. Suzuki, J. Magn. Magn. Mater. 161 (1996) 118.
[150] S. Wirth, M. Wolf, A. Margarian, K.-H. Müller, Proceedings of the Ninth International Symposium on Magnetic Anisotropy and Coercivity in Rare-Earth Transition Metal Alloys, World Scientific, Singapore, 1996, p. 399.